



HAL
open science

Kinematics of the local universe. VIII. Normalized distances as a tool for Malmquist bias corrections and application to the study of peculiar velocities in the direction of the Perseus-Pisces and the Great Attractor regions

G. Theureau, Stéphane Rauzy, L. Bottinelli, L. Gouguenheim

► To cite this version:

G. Theureau, Stéphane Rauzy, L. Bottinelli, L. Gouguenheim. Kinematics of the local universe. VIII. Normalized distances as a tool for Malmquist bias corrections and application to the study of peculiar velocities in the direction of the Perseus-Pisces and the Great Attractor regions. *Astronomy & Astrophysics - A&A*, 1998, 340, pp.21-34. hal-01704535

HAL Id: hal-01704535

<https://hal.science/hal-01704535v1>

Submitted on 30 Apr 2021

HAL is a multi-disciplinary open access archive for the deposit and dissemination of scientific research documents, whether they are published or not. The documents may come from teaching and research institutions in France or abroad, or from public or private research centers.

L'archive ouverte pluridisciplinaire **HAL**, est destinée au dépôt et à la diffusion de documents scientifiques de niveau recherche, publiés ou non, émanant des établissements d'enseignement et de recherche français ou étrangers, des laboratoires publics ou privés.

Kinematics of the local universe

VIII. Normalized distances as a tool for Malmquist bias corrections and application to the study of peculiar velocities in the direction of the Perseus-Pisces and the Great Attractor regions

G. Theureau^{1,2}, S. Rauzy⁴, L. Bottinelli^{1,3}, and L. Gouguenheim^{1,3}

¹ Observatoire de Paris/Meudon, ARPEGES/CNRS URA1757, F-92195 Meudon Principal Cedex, France

² Osservatorio Astronomico di Capodimonte, Via Moiariello 16, I-80131 Napoli, Italy

³ Université Paris-Sud, F-91405 Orsay, France

⁴ Centre de Physique Théorique - C.N.R.S., Luminy Case 907, F-13288 Marseille Cedex 9, France

Received 14 January 1998 / Accepted 8 September 1998

Abstract. We present a new method of bias correction for deriving reliable Tully-Fisher distances in a magnitude or diameter selected sample of field galaxies.

This normalized distance method (NDM) is first presented in a theoretical way using the formalism of bayesian statistics and is further applied to three different Tully-Fisher samples corresponding to three different passbands in *B*, *I* and *r*. Constraints imposed by the method, and influences of underlying assumptions and measurement errors are discussed in detail.

A main feature of the methodology is to extract an unbiased subsample from the parent sample. We show that by taking into account all the components influencing the bias at a given distance, the NDM method allows to extend the unbiased range and to analyze peculiar velocities of galaxies within a sphere out to 8000 km s⁻¹ around the Local Group.

Finally, thanks to this tool, we show first evidences for both frontside and backside large amplitude infall toward the Perseus-Pisces supercluster. The strong convergent flow expected in the Great Attractor region is not confirmed, even if infall centers are detected in this direction. The observed velocity field rather corresponds to the cumulative pull of several clusters present in this sky area.

Key words: galaxies: spiral – galaxies: distances and redshifts – cosmology: distance scale

1. Introduction

This paper takes place in a series which intends to study the kinematics of the Local Universe by using the Tully-Fisher relation (hereafter TF) as a distance indicator. Our research programme has required numerous stages from data acquirement to statistical and physical study of the distance criterion: in paper I and II (Bottinelli et al. 1992, 1993), we have presented a set of 600

new redshift measurements; in paper III (Paturel et al. 1994), we have discussed the completeness of our large *B*-band KLUN TF sample (see Sect. 2); in paper IV (Theureau et al. 1997a), we have shown evidence for a morphological type dependence of the TF zero point and explained this behaviour in terms of mass-luminosity structure; in paper V (Theureau et al. 1997b), we have calibrated the direct TF relation and obtained a firm value of the Hubble constant ($H_0=55$ km s⁻¹ Mpc⁻¹) from an unbiased sample of 400 field spiral galaxies; in particular, we have shown that this value depends only on the primary calibration given by the Period-Luminosity relation of cepheids and is in perfect agreement up to $z=0.1$ with the result given by SNIa standard candles; in paper VI (Theureau 1998), we have shown that the use of the mean surface brightness as an additional parameter allows us to reduce the scatter of the *B*-band TF relation by 30%, and then to reduce both distance uncertainties and statistical biases; hence, in paper VII (Theureau et al. 1998a) were presented the data of our 2700 galaxies HI-observational programme. On the basis of this careful step by step analysis, we are now able to study peculiar velocities at the scale of the Local Universe, i.e. for radial velocities up to 8000 km s⁻¹.

We discuss herein a new application of the normalized distance method (hereafter NDM), whose main principle was early presented by Bottinelli et al. (1986, 1988). Our main goal is the building of a reliable method for correcting TF distances from selection or Malmquist-like biases. In its most complete and updated form (Theureau et al. 1997b, Theureau 1998), the NDM method takes into account all observable astrophysical parameters influencing the selection bias: i.e. the redshift, maximum of rotational velocity $\log V_m$, magnitude or diameter completeness limit, internal and Galactic extinction corrections, morphological type, and mean surface brightness. The NDM method has proved to be an optimal tool for controlling accurately the behaviour of this bias against distance.

We recall that the selection bias we are discussing here is different from the bias described by Malmquist in his 1920's paper, which can be understood essentially as a geometrical ef-

Send offprint requests to: Gilles Theureau,
(theureau@cerere.na.astro.it)

fect. It has appeared in the literature under the following names: "Problem I" (Kapteyn, 1914), "Selection effect" (Han, 1992), "Distance-dependent bias" (Sandage, 1994), "Selection bias" (Strauss & Willick, 1995), and "Malmquist bias of the second kind" (Teerikorpi, 1997). However, as well shown by Teerikorpi (1997), this selection bias can be also understood as a parent of the classical Malmquist bias, both referring to two opposite points of view: we face a selection bias when we are concerned with the average TF distance at a fixed true distance (e.g. a given redshift); we face a geometrical bias when we are concerned with the average true distance at a given TF distance (e.g. a given observed couple $(B_t, \log V_m)$). When estimating a correction term, one has to choose either the former or the latter point of view, remembering that both have their advantages and their disadvantages. In the former case, a strictly magnitude complete or diameter complete sample is required for controlling the selection, i.e. one has to throw away an important part of the sample. On the other hand, no assumption is required about the spatial density distribution of the objects, and the uncertainty on corrected TF distance moduli decreases naturally as the distance increases, as a consequence of the magnitude or diameter cut off. In the latter case, no assumption is needed in terms of magnitude or diameter completeness (the whole sample may thus be used), but the spatial distribution has to be known (or assumed uniform) as well as the precise value of the TF scatter (in the uniform case, the bias $\Delta d/d$ is proportional to σ_{TF}), and the uncertainty on distances remains large ($\epsilon_d/d \propto \sigma_{TF}$).

In principle, by applying the appropriate normalization along the redshift scale, the NDM method allows to extract from the data the largest unbiased subsample as possible. By unbiased subsample we mean that for a set of galaxies at a given "true distance" (or at a given redshift or kinematical distance), the average TF distance of the group returns this true distance. Furthermore, under a restricted set of conditions, we show below that the bias can be expressed analytically as a function of only one parameter: the normalized distance $d_n = f(cz, \log V_m, m_{lim}, a_g, a_i, T, \Sigma)$ (see Sect. 3, and Eqs. 1 and 2). It thus becomes possible to construct a bias corrected set of distances that extends farther and contains much more objects than the strictly unbiased range: about 50% of the parent sample is usable (the strictly magnitude complete or diameter complete part of the sample), while only 10-20% can be kept in a purely unbiased subsample (equivalent to a volume complete subsample for each $p = \log V_m$). In addition, while the unbiased part is well populated only up to $cz \sim 3\text{-}4000 \text{ km s}^{-1}$, the bias corrected sample reaches the deepness of the parent catalogue, i.e. $cz \sim 8000 \text{ km s}^{-1}$. This corrected sample allows the study of the peculiar velocity field over large scales, in particular in the vicinity of some interesting region such as the Perseus-Pisces supercluster (PP) or the putative so-called Great Attractor (GA).

In this paper, the method is applied to three independent samples: our KLUN B -band TF-sample (6600 spirals distributed on the whole sky), the I -band TF-sample from Mathewson et al. (1992a) (1355 spirals in the Southern sky) and the r -band TF-sample from Willick (1991) (320 galaxies in the Perseus-Pisces region).

The values used for the direct TF slope and zero-point in B -band are those calibrated by Theureau 1998, using as primary calibrators a set of 15 pure cepheid extragalactic distances. In agreement with this previous study, the TF zero-point $b(\Sigma)$ is a function of the mean surface brightness Σ of the galaxies. By taking into account this dependence, the TF scatter was shown to be reduced by 30%, which is an important improvement when considering the Malmquist and selection bias effects as discussed further. I -band and r -band TF parameters have been derived in a separate paper by Theureau et al (1998b).

The mathematical formalism and notations refer to a series of papers by S.Rauzy, R.Triay, and M.Lachièze-Rey (Triay et al. 1994, Rauzy&Triay 1996, Triay et al. 1996, Rauzy 1997) devoted to the statistical analysis of the TF relation. We show that the normalized distance method can be fully described and understood in this context.

Main characteristics of the galaxy samples are summarized in Sect. 2. In Sect. 3, we describe theoretically the (NDM) method, using the mathematical formalism of probability densities. The empirical test of the plateau (see Theureau et al. 1997b) is presented as a statistical test of the method and of the assumptions used. Special attention is paid to the influences of the underlying hypothesis, measurement errors and parameter corrections. Sect. 4 is devoted to the construction of the corrected samples, to their properties, and to the constraints that the correction method imposes on further steps of the analysis. In Sect. 5, we give some examples of kinematical studies in the vicinity of some great mass concentrations such as the Perseus-Pisces (PP) region, and the controverted Great Attractor (GA). Sect. 6 finally contains elements of discussion on possible applications and prospects.

2. Data

The KLUN sample currently contains 6620 spiral galaxies having measured isophotal diameter D_{25} , HI line width, radial velocity, and also partially (6158) B -magnitudes. The sample was selected according apparent diameter; it is complete down to $D_{25} = 1.6$ arcmin (see Paturel et al. 1994 for a detailed study of the sample completeness) and covers the type range Sa-Sdm ($T=1\text{-}8$). The data were extracted from LEDA (see e.g. Paturel et al. 1997b) and complemented by our own observations (~ 600 optical and ~ 2250 HI spectra) with ESO and OHP optical telescopes, and Nançay and Parkes radiotelescopes (Bottinelli et al. 1992, 1993, di Nella et al. 1996, Theureau et al. 1998a). They have been reduced to a standard and common system according to Paturel et al. (1991, 1997a, 1997b) for photometric data and Bottinelli et al. (1990) for HI data. Isophotal D_{25} diameters and apparent B -magnitudes are corrected for galactic extinction according to Fouqué&Paturel (1985), and for inclination effect (i.e. opacity effect) in agreement with Bottinelli et al. (1995). Errors on apparent magnitude are less than 0.4 mag, while errors on apparent diameter are less than 0.115 arcmin. HI line widths, reduced to the standard levels of 20% and 50%, are corrected for internal velocity dispersion according to Tully&Fouqué (1985). We recall that the observational errors

on astrophysical parameters are computed in LEDA by taking into account both the quality of individual measurements and the standard deviation of these measurements from a weighted mean.

The *I*-band Mathewson, Ford, and Buchhorn (1992a) sample (hereafter MFB) contains 1355 spiral galaxies (SO-Sm) distributed in the Southern hemisphere. Accurate CCD photometry was obtained in the Kron-Cousins *I*-passband. According to the authors, the error in magnitude is less than 0.1 mag ($\simeq 0.03$ on average). Extinction in *I* was taken to be 42% of that in *B* (using Burstein&Heiles 1984 system), and K-corrections were taken from Schneider, Gunn, and Hoessel (1983). The sample is complete in magnitude up to $I=12.5$ mag (see e.g. Federspiel et al., 1994). Maximum of rotational velocity parameter ($\log V_m$) were mainly derived from H_α rotation curves (for 965 objects) obtained with a dual beam spectrograph attached to the 2.3 m telescope. The resolution is 18 km s^{-1} per pixel at H_α . These observations were complemented with 21-cm line widths obtained with the 64 m radiotelescope of Parkes Observatory (551 objects). The HI spectral resolution after smoothing is 7 km s^{-1} .

The whole sample compiled by Willick (1991) contains 320 spiral galaxies of the Perseus-Pisces region (hereafter W91PP). It covers a small area on the sky, restricted to the main filamentary structure of the supercluster, and extends in radial velocity from $cz \sim 3000 \text{ km s}^{-1}$ to $cz \sim 8000 \text{ km s}^{-1}$. The photometric data were carried out through a red filter centered on $\lambda=0.67 \mu\text{m}$ (*r*-band). The sample appears complete in magnitude up to $r=14.3$ mag. Extinction in *r* was taken to be 60% of that in *B* (using Burstein&Heiles 1984 system), and K-corrections were taken from Schneider, Gunn, and Hoessel (1983). HI line widths, obtained with Arecibo radiotelescope, were got from Giovanelli&Haynes (1985) and Giovanelli et al. (1986).

For the three samples, heliocentric radial velocities are corrected to the centroid of the Local Group according to Yahil et al. (1977). A kinematical distance scale d_{kin} is built assuming an infall velocity of the Local Group toward the Virgo cluster $v_0 = 150 \text{ km s}^{-1}$ and an observed radial velocity of Virgo $(V_0)_{Vir} = 980 \text{ km s}^{-1}$ (Mould et al. 1980) and using Peebles's linear infall model (1976). Galaxies close to the galactic plane ($|b| \leq 15^\circ$ for KLUN galaxies, $|b| \leq 10^\circ$ for MFB galaxies) are excluded because of too large uncertainties in the galactic extinction correction (see Paturel et al. 1997b). Face-on galaxies ($\log R_{25} < 0.07$) are excluded because of the larger error on $\log V_m$. We excluded also too close objects and those belonging to the "triple value region" around the Virgo core because of the large uncertainties on their kinematical distance.

Finally, for fulfilling the condition *H3* of Sect. 3.3, the three samples are strictly cut off at their completeness limit, i.e. at $\log D_{25,lim}=1.2$ (D_{25} expressed in 0.1 arcmin) for KLUN, $I_{lim}=12.5$ mag for MFB, and $r_{lim}=14.3$ for W91PP. After these restrictions, we are left with 2454 galaxies for KLUN, 597 galaxies for MFB, and 167 galaxies for W91PP (see Figs. 7-9).

3. Statistical approach

3.1. Problematic

The use of the Tully-Fisher relation is based on several parameters which appear in a statistical model as random variables. These variables are listed below:

- the absolute magnitude M
- the logarithm of the absolute or linear diameter $\log D$
- the apparent magnitude m in a given passband
- the logarithm of the photometric diameter $\log D_{25}$
- the intrinsic parameter $p = \log V_m$, where V_m is the maximum of rotational velocity obtained either directly from rotation curves or derived from the 21-cm line width
- the distance modulus $\mu = 5 \log r + 25$ (with the distance r in Mpc). Thus $\mu = 5(\log D - \log D_{25}) + 25 = m - M$
- the TF residual ζ_M or ζ_D , of zero mean and dispersion σ_{ζ_M} or σ_{ζ_D} equal to the TF intrinsic dispersion, which account for intrinsic error in the TF relations

$$-M = a_M p + b_M + \zeta_M \quad (\text{magnitude version})$$

$$\log D = a_D p + b_D + \zeta_D \quad (\text{diameter version})$$

Assuming that there is no evolution effect for the galaxy population investigated (i.e. neither M nor D depends on the distance modulus μ) and that the N galaxies of the sample are independent events, the probability density dP_M (for the magnitude relation) or dP_D (for the diameter relation) of a sampled galaxy is expressed as follows:

$$dP_M \propto \Psi(m, p, \mu) F(M, p) dM dp h(\mu) d\mu f(v, \mathbf{x}) dv$$

$$dP_D \propto \Psi(\log D_{25}, p, \mu) F(\log D, p) d(\log D) dp$$

$$\times h(\mu) d\mu f(v, \mathbf{x}) dv$$

Where:

- $F(M, p)$ (resp. $F(\log D, p)$) is the distribution function of the coupled variables (M, p) (resp. $(\log D, p)$)
- $h(\mu)$ is the spatial density distribution function along the line-of-sight pointing toward galactic coordinates (l, b)
- $\Psi(m, p, \mu)$ is the selection function applied to the sample; it takes into account the actual observational selection of the sample, and possible choices of subsampling related to the method of analysis
- $f(v, \mathbf{x})$ is the spatial distribution function of peculiar velocities; it generally depends on the spatial position of the galaxy $\mathbf{x} = (r \cos l \cos b, r \sin l \cos b, r \sin b)$

The characteristics of these functions motivate the choice of working hypotheses and so determine the method of analysis. In particular, constraints are different if one wants to calibrate the TF relation in the field or in a cluster, calculate H_0 , or compute the peculiar velocity field from individual TF distances.

3.2. Normalized distance method and plateau technique

The normalized distance method was first elaborated by Bottinelli et al. (1986), and updated in its complete form by Theureau et al. (1997b). The original aim of this semi-empirical method was to extract an unbiased subsample from the data of a strictly magnitude or diameter limited sample, in the most rigorous and efficient way. We will show further that, since it is possible to predict the general behaviour of the selection bias as a function of the normalized distance, it becomes natural to extrapolate the unbiased range and to build, for a given parent sample, an intrinsic correction method of TF distances.

Obviously, due to the existence of a completeness limit, in magnitude or in diameter, for any sample of galaxies, the luminosity or size distribution function of the objects present in the catalogue (e.g. corresponding to a given value of the intrinsic parameter p) is fully traced by the sample only up to a fixed distance limit. Above this limit, the distribution function (or the distribution of the TF residuals) is truncated in its fainter part, and the average luminosity or size of the objects sampled no more corresponds to the value set by the TF relation. This effect results in a progressive under-estimation of derived distances. Moreover, the distance limit, or the shape of the bias curve against distance, not only depends on p , σ_{TF} and the magnitude (or diameter) limit, but also on the Galactic extinction and opacity, and on the morphological type and the mean surface brightness of the objects. The normalized distance method allows to treat all these influences in a coherent way.

The normalized distance d_n is defined as follows:

$$d_n = d_{\text{kin}} \cdot 10^{0.2a_M(2.7 - \log V_m)} \cdot 10^{0.2a_i(\log R_{25}, T)} \cdot 10^{0.2a_g} \cdot 10^{0.2(m_0 - m_{\text{lim}}(T))} \cdot 10^{-0.2(b(T) - b(6))}, \quad (1)$$

for the magnitude relation, and for the diameter relation

$$d_n = d_{\text{kin}} \cdot 10^{a_D(2.7 - \log V_m)} \cdot 10^{-C \log R} \cdot 10^{0.094a_g} \cdot 10^{(\log D_{\text{lim}} - \log D_0)} \cdot 10^{-(b(T) - b(6))}, \quad (2)$$

where a_M or a_D is the TF slope; the factor $a_i(\log R_{25}, T)$ or the constant C takes care of the influence of the opacity correction on the observed magnitude or diameter; the term in a_g is the extinction correction; the term in m_{lim} or D_{lim} accounts for the catalog limit and its variations with the morphological type; the term with $b(T)$ takes care of the TF zero-point variation with morphological type (it can be replaced by $b(\Sigma)$ when considering rather the mean surface brightness dependence); and $d_{\text{kin}} = V/V_{\text{Virgo}}$ is the kinematical distance in units of the Virgo cluster distance (see Sect. 2).

The technique consists in replacing, in the diagram $\log H = \log(V/d_{TF})$ vs. d , the distance d by the normalized distance d_n using the above formulae. The bias curves $\langle \log H \rangle(d)$ corresponding to the various classes of objects (different $\log V_m$, different inclination, different Galactic latitude, different morphological type or mean surface brightness) are then superimposed, and the bias effect $\langle \log H \rangle(d) - \log H_0$ is only a function of the normalized distance. Doing so, the unbiased subsample appears as a plateau in this diagram (see figs. 1 and 2), provided

the sample is complete either in magnitude or diameter. The consistency of this method depends on the good knowledge of the completeness limit, and on the influence of peculiar velocities on the sharpness of the plateau limit. These aspects are discussed in the next subsection.

3.3. Formal analysis

The direct (i.e. forward) TF relation is characterized by the independency of the residuals ζ with respect to the p parameter (the covariance $\text{Cov}(p, \zeta)$ is assumed equal to zero). In the case of the magnitude TF relation, it implies that the function $F(M, p)$ rewrites $F(M, p)dMdp = f_p(p)g(\zeta)dpd\zeta$, where $f_p(p)$ is the distribution function of the variable p and $g(\zeta)$ is the distribution of residuals. One gets the same kind of formula in the case of the diameter TF relation.

We now consider the following hypothesis:

- *H1* : the radial velocity field V obtained after subtraction of a peculiar velocity field model $V_p(\mathbf{x})$ (herein the Virgo infall) reduces to a pure Hubble flow.

$$V = cz - V_p(\mathbf{x}) = H_0 r \quad (3)$$

- *H2* : the global selection function $\Psi(m, p, \mu)$ can be split into $\Psi(m, p, \mu) = \psi_m(m)\psi_{p,\mu}(p, \mu)$
- *H3* : the sample is complete and strictly magnitude limited (i.e. $\psi_m(m) = \theta(m_{\text{lim}} - m)$ with $\theta(x)$ the Heaveside or step function).
- *H4* : the distribution function $g(\zeta)$ is a gaussian of zero mean and constant dispersion σ_ζ equal to the standard deviation σ_{TF} of the TF relation

$$g(\zeta) \equiv g_G(\zeta; 0, \sigma_\zeta) = \frac{1}{\sqrt{2\pi} \sigma_\zeta} \exp\left[-\frac{(\zeta - 0)^2}{2\sigma_\zeta^2}\right] \quad (4)$$

Under these assumptions, the probability density of a sampled galaxy reads as follows:

$$dP = \frac{1}{A} \theta(m_{\text{lim}} - m) \psi_{p,\mu}(p, \mu) f_p(p) g_G(\zeta) dp d\zeta h(\mu) d\mu \quad (5)$$

where A is the normalization factor warranting $\int dP = 1$.

3.3.1. Bias correction

Let us now express dP for a subsample of galaxies having the same normalized distance $d_n = d_0$. By using definition of Eq. (1) and assumption H1 of Eq. (3), d_n may be written in its most simple form as:

$$5 \log d_n = (\mu - a_M p + a_M p_0) + Cte_1 = m + \zeta + Cte \quad (6)$$

where influences of opacity, extinction and type or brightness may be understood as variations of the magnitude limit m_{lim} or variations of the normalisation constant p_0 . At this stage, it is convenient to introduce the function $\omega(d)$:

$$\omega(d) = 5 \log d - Cte \quad (7)$$

such that $d_n = d_0$ implies $m + \zeta = \omega(d_n) = \omega(d_0) = \omega_0$. Applying conditional probability to Eq. (5), the probability density dP_{d_0} of a sample at a given normalized distance d_0 reads:

$$dP_{d_0} = \frac{1}{A_{d_0}} \theta(\zeta - (\omega_0 - m_{lim})) g_G(\zeta; 0, \sigma_\zeta) d\zeta \times J(p) dp \quad (8)$$

with $J(p) = \psi_{p,\mu}(p, \omega_0 + ap + b) f_p(p) h(\omega_0 + ap + b)$ and A_{d_0} the normalization factor:

$$A_{d_0} = \int_{\omega_0 - m_{lim}}^{+\infty} g_G(\zeta; 0, \sigma_\zeta) d\zeta \times \int_{-\infty}^{+\infty} J(p) dp$$

This is mind, one can now calculate the average bias on the random variable $\log H = \log(V/d_{TF})$ as a function of the normalized distance d_n . The rough TF distance modulus estimate μ_{TF} is defined as:

$$\mu_{TF} = 5 \log d_{TF} + 25 = m + a_M p + b_M \quad (9)$$

Following assumption H1, $\log H$ thus reads:

$$\log H = \log V - \log d_{TF} = \log H_0 + 0.2 \zeta \quad (10)$$

It implies that, for a given normalized distance $d_n = d_0$, one gets $\langle \log H \rangle(d_0) = \log H_0 + 0.2 E(\zeta)$ with $E(\zeta)$ the mathematical expectancy of ζ at a given d_0 (i.e. $E(\zeta) = \int \zeta dP_{d_0}$). The calculation gives ¹:

$$E(\zeta) = C(\omega_0) = 2\sigma_\zeta^2 \frac{\frac{1}{\sqrt{2\pi}\sigma_\zeta} \exp\left(-\frac{(\omega_0 - m_{lim})^2}{2\sigma_\zeta^2}\right)}{1 + \text{erf}\left(\frac{\omega_0 - m_{lim}}{\sqrt{2}\sigma_\zeta}\right)} \quad (11)$$

where $\text{erf}(x) = \frac{2}{\sqrt{\pi}} \int_0^x \exp(-t^2) dt$. It thus turns out that if hypotheses H1, H2, H3 and H4 are satisfied by the sample, the averaged $\log H$ by bins of normalized distance d_n verifies:

$$\langle \log H \rangle(d_n) = \log H_0 + 0.2 C(\omega(d_n)) \quad (12)$$

where functions ω and C are respectively defined Eq. (7) and Eq. (11). We thus expect first a plateau at short distances (i.e. at d_n such that $\omega(d_n) - m_{lim} \ll \sigma_\zeta$) corresponding to $\langle \log H \rangle \simeq \log H_0$, followed by a progressive divergence of $\log H$ from this plateau as d_n increases (see Fig. 1).

Note that the term $0.2 C(\omega(d_n))$ involved in the quantity $\langle \log H \rangle(d_n)$ of Eq. (12) appears in fact as a bias correction. It suggests to introduce the following bias corrected quantity as a distance indicator:

$$\tilde{\mu}_{ND} = \mu_{TF} + C(\omega(d_n)) = m + a_M p + b_M + C(\omega(d_n)) \quad (13)$$

where $C(\omega(d_n))$ has to be understood as an averaged correction term, at a given normalized distance d_n , for the rough TF distance modulus estimate μ_{TF} . For a subsample of galaxies with the same d_n , one can check that the distance modulus estimator $\tilde{\mu}_{ND}$ verifies $E(\tilde{\mu}_{ND} - \mu | d_n) = 0$ (i.e. the average of the $\tilde{\mu}_{ND}$'s coincides with the mean true distance modulus $\langle \mu \rangle$ of the sample. This unbiased distance modulus estimator will be used hereafter Sects. 4 and 5 as a starting point for kinematical analyses.

¹ The form of the function C herein defined is comparable to the expression of the "average bias at a given true distance" as calculated by Teerikorpi (1984), assuming a gaussian luminosity function and a gaussian distribution of the residuals of the inverse TF relation.

3.3.2. The unbiased plateau

In practice, the extraction of the unbiased plateau (cf. Sect. 3.2.) is performed through the following subsampling. For a given value of p , the cut-off in absolute magnitude $M_{lim} = m_{lim} - \mu$ should not be closer than $3\sigma_\zeta$ to the mean $-M(p) = a_M p + b_M$. It corresponds to add the following extra selection function to $\psi_{p,\mu}(p, \mu)$:

$$\psi_{p,\mu}(p, \mu) = \theta(M_{lim} - 3\sigma_\zeta - M(p)) \phi_{p,\mu}(p, \mu) \quad (14)$$

Such a subsampling is equivalent to a selection in normalized distance d_n , e.g. $d_n \leq d_0$ with $\omega(d_0) = m_{lim} - 3\sigma_\zeta$:

$$\psi_{p,\mu}(p, \mu) = \theta(m_{lim} - 3\sigma_\zeta - m - \zeta) \phi_{p,\mu}(p, \mu) \quad (15)$$

where Eqs. (6,7) have been used. We now remark that the first factor $\theta(m_{lim} - 3\sigma_\zeta - m - \zeta)$ in the above expression is more stringent (e.g. at 3σ) than the apparent magnitude sample selection $\psi_m(m) = \theta(m_{lim} - m)$. It thus turns out that the global selection function of the unbiased plateau can be expressed as follows:

$$\Psi_{pl}(m, p, \mu) = \theta(m_{lim} - m) \psi_{p,\mu}(p, \mu) \simeq \psi_{p,\mu}(p, \mu) \quad (16)$$

and the probability density of Eq. (5) for a galaxy belonging to the plateau rewrites as:

$$dP_{pl} \simeq \frac{1}{A_{pl}} \psi_{p,\mu}(p, \mu) f_p(p) h(\mu) dp d\mu \times g_G(\zeta; 0, \sigma_\zeta) d\zeta \quad (17)$$

It implies that the sample constituted of plateau galaxies verifies the 3 following properties:

$$E(\zeta) \simeq 0 \quad (\text{a}); \quad \text{Cov}(p, \zeta) \simeq 0 \quad (\text{b}); \quad \text{Cov}(\mu, \zeta) \simeq 0 \quad (\text{c}). \quad (18)$$

Note that these 3 properties are valid whatever the specific shape of the functions $h(\mu)$, $f_p(p)$, and $\phi_{p,\mu}(p, \mu)$, i.e. respectively the distribution of galaxies along the line-of-sight, the distribution function of the p 's, and the observational selection in p and distance modulus μ .

Property (18a) results from the fact that residuals ζ follow a distribution centered on 0. We remark that, according to Eqs. (11,12), one obtains $\langle \log H \rangle \simeq \log H_0$ for the plateau galaxies. Property (18b) permits the estimation of the direct TF slope a_M by means of a least square direct TF regression. These results constitute the theoretical basis of the normalized distance method used by Bottinelli et al. (1986), Theureau et al. (1997a, 1997b) and Theureau (1998).

Finally, when used with the appropriate selection function, the plateau method consists in selecting a set of data for which the covariance $\text{Cov}(\mu, \zeta)$ is zero (property (18c)), or in other words, for which the TF residuals are independent of the distance. Consequently, the plot of $\text{Cov}(\mu, \zeta)$ as a function of $d_{n,lim}$ (the plateau limit adopted) provides us with a statistical test of the method, i.e. of the selection of the unbiased range, and then a test of the actual completeness of the sample (in magnitude or in diameter) as required from the hypothesis H3. The method provides us also with a test of the velocity field model used to correct radial velocities from the Virgo infall component:

the dispersion $\sigma(\log H)$ is minimized when the correct parameters V_{GL} and V_{Virgo} are used (cf Sect. 2). An application, leading to $V_{GL}=200 \pm 30 \text{ km s}^{-1}$, may be found in Theureau et al. (1997b). Influences of assumptions and measurement errors are discussed in the following subsection.

3.4. Checking of observational errors and assumptions

The least square direct TF regression supposes that all errors are along the magnitude (resp. diameter) axis, i.e. that the slope a of the TF relation is calculated by solving the equation $\text{Cov}(p, \zeta) = 0$. Because there are only a few primary calibrators available ($\simeq 20$ extragalactic cepheid distances), the slope is estimated using field galaxies, assuming that the kinematical distance scale (modulo H_0 and corrected for a Virgo infall component) provides us with a satisfying relative distance scale.

From $\text{Cov}(p, \zeta) = 0$, one gets for the magnitude relation the slope:

$$a_M = \frac{\text{Cov}(p, \mu) - \text{Cov}(p, m)}{\text{Cov}(p, p)} \quad (19)$$

or, for the diameter relation:

$$a_D = \frac{\text{Cov}(p, 5 \log D_{25}) + \text{Cov}(p, \mu)}{5 \text{Cov}(p, p)} \quad (20)$$

where $\mu = 5 \log cz + \text{const.}$

3.4.1. Influence of the peculiar velocity field

We have calculated the TF slope and estimated the unbiased range limit, assuming in first approximation that the velocity field is described by a pure Hubble flow. Hereafter the measured radial velocity cz is decomposed as follows:

$$cz = H_0 r + V_p + \varepsilon_v \quad (21)$$

where $H_0 r$ is the pure expansion component, V_p is the sum of contributions of systematic peculiar motions due to the gravitational environment (Local Anomaly, Virgo infall, Great Attractor, constant field, ...), and ε_v takes into account both a random velocity component and measurement errors (ε_v is assumed to be described by a gaussian law centered on 0, with a standard deviation σ_{ε_v}). The observed kinematical distance modulus $\hat{\mu} = 5 \log cz - 5 \log H_0 + 25$ is then related to the true distance modulus μ as follows:

$$\hat{\mu} = \mu - \frac{1}{\alpha} \ln\left(1 - \frac{V_p + \varepsilon_v}{cz}\right) \approx \mu + \frac{1}{\alpha} \frac{V_p + \varepsilon_v}{cz} + \dots \quad (22)$$

where $\alpha = 0.2 \ln 10$ and the last term is the approximation of the formula at its first order (this approximation will be hereafter considered as a fair one).

Then, the presence of peculiar velocities influences slope estimation as well as plateau limit. The measured TF slope \hat{a} is related to the true one by the following formula:

$$\hat{a} \approx a + \frac{1}{\alpha} \frac{\text{Cov}(p, \frac{V_p + \varepsilon_v}{cz})}{\text{Cov}(p, p)} \quad (23)$$

The additional term is roughly zero, if we exclude from the sample galaxies close to the center of rich clusters, where peculiar motions are more important, and where tidal effects may change the internal dynamics and the neutral hydrogen gas distribution in the disc.

For the plateau condition, we get:

$$\text{Cov}(\hat{\mu}, \zeta) \approx \text{Cov}(\mu, \zeta) + \frac{1}{\alpha^2} \text{Cov}\left(\frac{V_p + \varepsilon_v}{cz}, \frac{V_p + \varepsilon_v}{cz}\right) \quad (24)$$

Note that the influence of peculiar velocities (right term) is reduced when:

- 1) a velocity field model is used to correct for the Virgo infall: with the right infall parameters V_{GL} and $(V_0)_{Vir}$, $\left|\frac{V_p + \varepsilon_v}{cz}\right|$ is minimized.
- 2) peculiar velocities are small with respect to Hubble expansion: this is the case when galaxies with observed radial velocity smaller than 700 km s^{-1} are excluded.

3.4.2. Measurement errors and their correlations

Hereafter variables with hat denote the measured variables while those without hat are the true ones:

- $\hat{\mu} = \mu + \varepsilon_\mu$ with $\varepsilon_\mu \approx \frac{1}{\alpha} \frac{V_p + \varepsilon_v}{cz}$ is due to the presence of peculiar velocities.
- $\hat{m} = m + \varepsilon_m$ where ε_m are the measurement errors on m (of dispersion σ_{ε_m}).
- $\hat{p} = p + \varepsilon_p$ where ε_p are the measurement errors on p (of dispersion σ_{ε_p}).

In the case of the direct TF relation, all errors are supposed to be on the magnitude axis; this is not true, even if the error ratio between the two axis, $\frac{\varepsilon_m + \frac{1}{\alpha} \frac{V_p + \varepsilon_v}{cz}}{a \varepsilon_p}$, favours this assumption. Note also that it is generally assumed that measurement errors on both axis are not correlated; this is not true either.

We know from Eq. (19) that the derived TF slope depends on the three following terms which can be developed as:

$$\begin{aligned} \text{Cov}(\hat{m}, \hat{p}) &= \text{Cov}(m, p) \\ &+ \text{Cov}(m, \varepsilon_p) + \text{Cov}(\varepsilon_m, p) + \text{Cov}(\varepsilon_m, \varepsilon_p) \end{aligned}$$

$$\begin{aligned} \text{Cov}(\hat{p}, \hat{\mu}) &= \text{Cov}(p, \mu) \\ &+ \text{Cov}(\varepsilon_p, \varepsilon_\mu) + \text{Cov}(p, \varepsilon_\mu) + \text{Cov}(\varepsilon_p, \mu) \end{aligned}$$

$$\text{Cov}(\hat{p}, \hat{p}) = \text{Cov}(p, p) + \text{Cov}(\varepsilon_p, \varepsilon_p) + 2\text{Cov}(p, \varepsilon_p)$$

The following points have then to be taken into account:

- $\text{Cov}(\varepsilon_m, \varepsilon_p) \neq 0$, because the inclination (or the axis ratio) of the galaxy is used both to correct $p = \log V_m$ for projection effect, and to correct magnitudes for internal extinction effect. However, in the case of the diameter relation, $\varepsilon_{\log D}$ is poorly correlated with ε_p , due to the very small opacity correction for apparent diameters (see Bottinelli et al. 1995), and the effect can be neglected.

- $\text{Cov}(\varepsilon_p, \varepsilon_p) = \sigma_{\varepsilon_p}^2$ differs from zero, the average of σ_{ε_p} over the whole sample is roughly 0.1; even if small, this effect has to be taken into account.
- $\text{Cov}(\varepsilon_p, \varepsilon_\mu) \neq 0$ because the measurement errors ε_p and ε_μ are correlated, both p and cz being carried out from the same HI profile. However, the influence of $\frac{\varepsilon_v}{cz}$ vanishes rapidly when the distance increases.
- $\text{Cov}(p, \varepsilon_\mu)$, $\text{Cov}(\mu, \varepsilon_p)$ and $\text{Cov}(p, \varepsilon_p)$ may not be null due to the coupled selection effects in p and μ .

3.4.3. On the assumption $\sigma_{TF}(p) = \text{const.}$

The use of the normalized distance method requires that the TF dispersion is constant whatever the value of $p = \log V_m$ (H4, Sect. 3.3.), but this is not necessarily true... Obviously, when in the case of the *B*-band TF relation no correlation is observed between TF residuals and the p parameter (Theureau et al. 1997b), there is a marginal correlation when the *r*-band is used (see Willick et al., 1997), and a significant effect in the case of the *I*-band TF relation (about 0.2 mag from slowest to fast rotators, see e.g. Theureau et al. 1998b). Giovanelli et al. (1997) showed that this component is mainly intrinsic and could result from variety of sources, such as "asymmetries in the spiral disks" light distribution and velocity field, and differences in the formation and histories of galaxies".

Such a systematically changing character of the TF scatter might have important effects in the estimates of our bias corrections. It first introduces some "fuzzyness" on the plateau selection, which then must be chosen more conservative. It also leads to larger uncertainties on derived peculiar velocities, which in the case of the *I*-band sample are slightly overestimated for small p and slightly under-estimated for large p . This may result in a second order systematic effect creating at large distances a spurious enhancement of the infall pattern in its backside (Sect. 5).

In more formal terms, because ζ^2 is correlated with p , the Eq. (8) which gives the normalization factor is no more verified. $E(\zeta)$ then cannot be calculated as in Eq. (11), since its value depends on the shape of $J(p)$, i.e. on the galaxy spatial distribution, on the p distribution function, and on the selection effects in p and μ . This means that, for using the *I*-band TF relation in a proper way, one should treat separately the different p ranges, provided a sufficiently large and statistically reliable sample. Finally, one notes that if the σ_ζ dependancy on p affects the definition of the plateau limit, it does not modify Eq. (17) and thus properties (18a,18b,18c); i.e. the calibration of TF slope and zero-point using plateau galaxies is insensitive to a TF scatter dependancy on p .

4. Corrected distances

We have shown in Sect. 3.2. that since the selection bias $\Delta\mu$ on the estimated TF distance modulus depends on the set of parameters (p , d_{kin} , $a_g(l, b)$, $a_i(\log R_{25}, T)$, T or Σ), it can be only expressed as a function of the normalized distance d_n . We recall that this is true only in the case of strictly magnitude

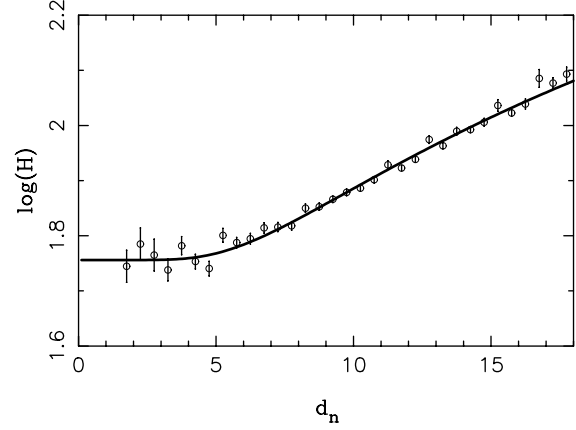


Fig. 1. $\log H$ vs. d_n diagram for the KLUN sample. Open circles represent the average value of $\log H$ for a series of d_n bins. Error bars denote the statistical error on this mean value. The full line fitted to the data is the theoretical bias curve, as obtained from Eq. (14).

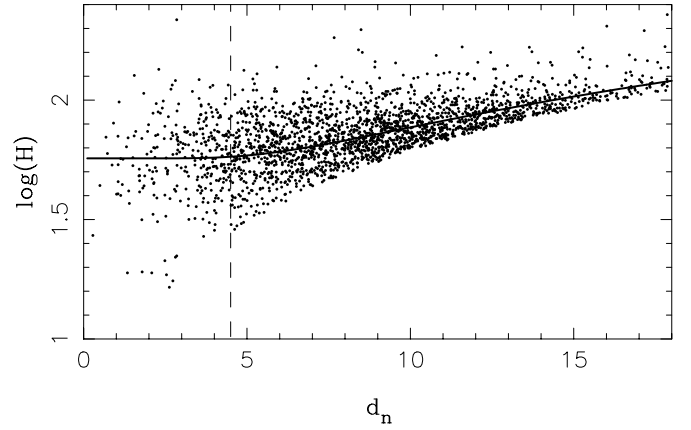


Fig. 2. $\log H$ vs. d_n diagram for the KLUN sample. Each point represents an individual galaxy. As in Fig. 1, the full line fitted is the theoretical bias curve, as obtained from Eq. (14).

complete or diameter complete sample. To this end, the samples are cut off at their completeness limit (see Sect. 2). In addition, due to the use of kinematical distances as a reference distance scale, it is also required that the integral over all the directions (l, b) of the function $f(v, \mathbf{x})$ describing the peculiar velocities is the unity, i.e. except the cosmic expansion there is no coherent velocity field at the scale of the sample. Such an hypothesis requires either a large sky coverage of the sample (typically as KLUN), or a reasonably deep survey, otherwise it is not possible to fit safely the theoretical bias curve to the data.

Using the normalized distance method, all the bias curves $\langle \log H \rangle(d_{kin})$ associated to the various parameters are superimposed in a unique curve $\langle \log H \rangle(d_n)$ traced by a function $\Delta H = 0.2C(\omega(d_n))$ where functions C and ω are defined Eqs. (11) and (7). Note that the bias ΔH is independent of the galaxy space distribution $h(\mu)$. Its general form, which takes into account all the parameters implied, requires to replace m_{lim} by the effective magnitude limit:

$$m_{lim,eff} = m_{lim}(T) - a_g(l, b) - a_i(\log R_{25}, T)$$

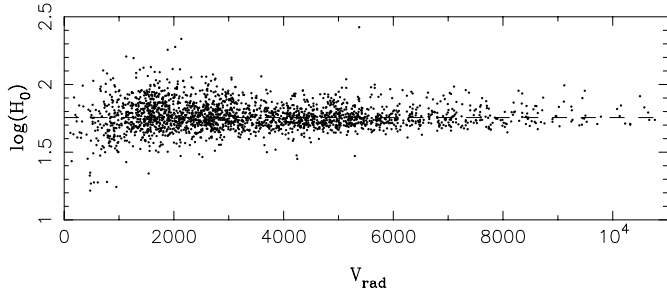


Fig. 3. $\log H$ vs. V_{rad} diagram for the corrected distance sample (KLUN).

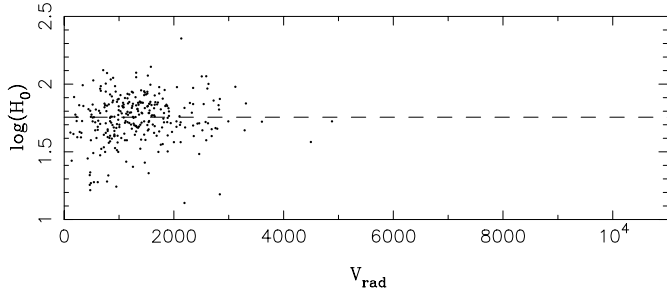


Fig. 4. $\log H$ vs. V_{rad} diagram for the unbiased sample only (KLUN).

And the normalisation term p_0 by:

$$p_{0,eff} = p_0 + \frac{1}{a}(b(T) - b(6))$$

or

$$p_{0,eff} = p_0 + \frac{1}{a}(b(\Sigma) - b(10.))$$

The corrected distance is finally given by the following equation:

$$\begin{aligned} \log d_{corr} &= \log d_{TF} + 0.2C(\omega(d_n)) = \\ &0.2(m + a_{TF}p + b_{TF} - 25) + 0.2C\left(5 \log d_{kin} + a(p - p_0) \right. \\ &+ a_g(l, b) + a_i(\log R_{25}, T) + (m_0 - m_{lim}(T)) \\ &\left. - (b(T) - b(6)) - 25\right) \end{aligned}$$

Figs. 1 and 2 show the bias curve ($\log H_0 + 0.2C(\omega(d_n))$) fitted to a series of average points $\langle \log H \rangle(d_n)$ and to individual points $(\log H, d_n)$ respectively, using the KLUN sample. Note the clear plateau region, at short normalized distance, which defines the unbiased range. For comparison, we plot in Figs. 3 and 4 the corrected sample and the extracted unbiased subsample in a $\log H$ vs. V_{rad} (radial velocity) diagram. As expected, $\langle \log H \rangle = \langle \log(V_{rad}/d_{TF}) \rangle$ appears now constant whatever the distance is, up to $V_{rad} \sim 8000 \text{ km s}^{-1}$, whereas the unbiased subsample is limited to $V_{rad} \sim 3000 \text{ km s}^{-1}$. Note in Fig. 2 the small set of galaxies lying at small $\log(H)$ (~ 1.3), clearly out of the main cloud of points. These galaxies have a radial velocity between 300 and 700 km s^{-1} and belong essentially

Mathewson Sample (I -band)

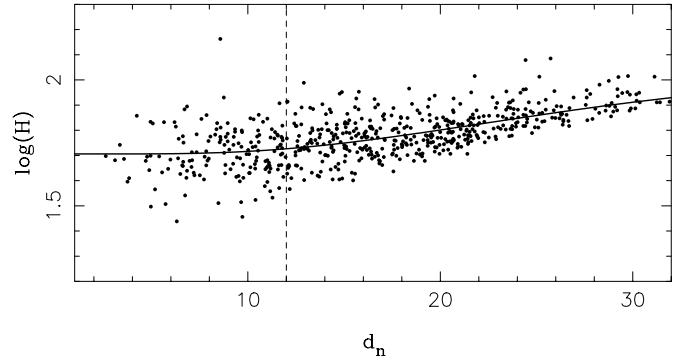


Fig. 5. As in Fig. 2, but for the MFB I -band sample

Willick 91 Sample (r -band)

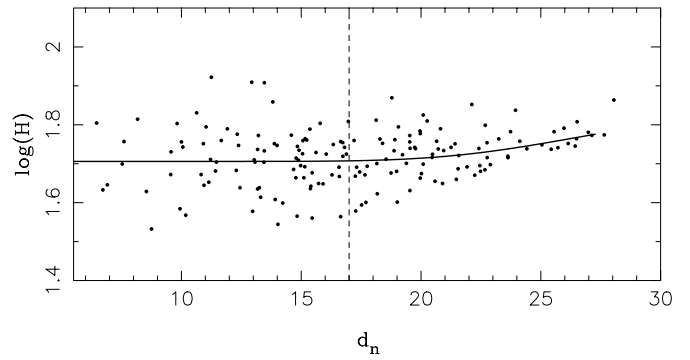


Fig. 6. As in Fig. 2, but for the W91PP r -band sample

to the Local (Coma-Sculptor) Cloud. They take part in the Local Anomaly, a local bulk flow discovered by Faber&Burstein (1988). Figs. 5 and 6 are the equivalent of Fig. 2, for the MFB and W91PP samples respectively. Due to the smaller dispersion of the TF relation in I and r , the unbiased range is deeper and the bias curve shallower than in B . However, the corresponding corrected distance samples are less populated and less deep than for our B -sample, and only a few objects are available at large distances.

the corrected distance sample contains 2454, 597, and 167 galaxies for the KLUN sample, the MFB sample, and the W91PP sample, respectively. The Aitoff projection of these three samples is displayed on Figs. 7, 8, and 9.

5. Toward a kinematical study of the Local Universe

5.1. V against d or d against V ?

There are two ways for investigating a V (velocity) vs. d (distance) diagram from the direct TF relation: the plot of V against d or of d against V . It was shown by Teerikorpi (1993) that both points of view hide some specific problems, and that special care is needed for interpreting such diagrams in the search for systematic peculiar motions. Difficulties are due to the large TF intrinsic scatter, which makes distance uncertainties large (15%

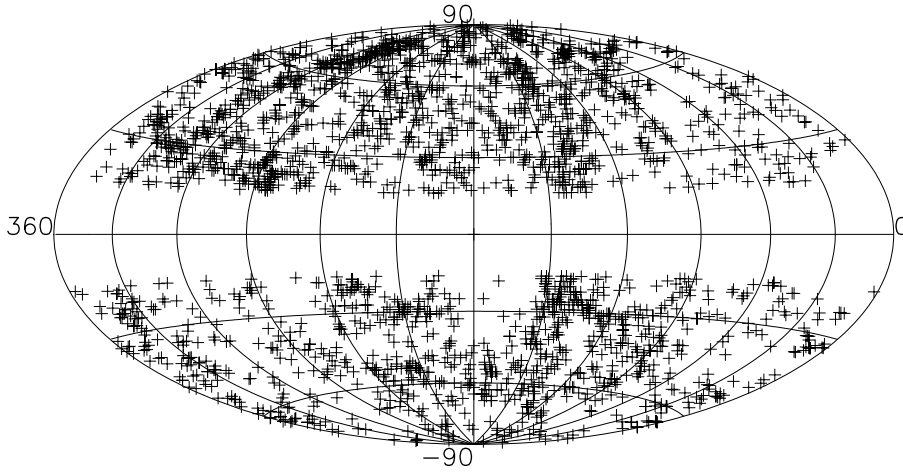


Fig. 7. Aitoff projection of the KLUN corrected distance sample in galactic coordinates (2454 galaxies)

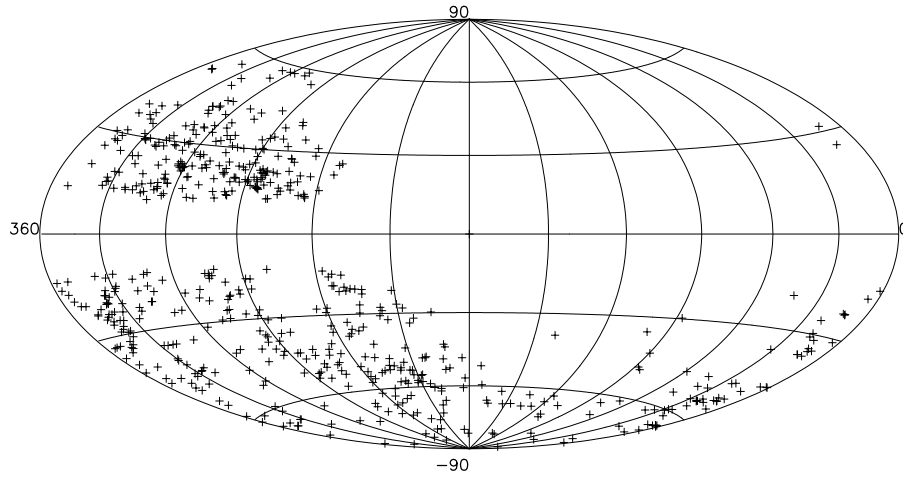


Fig. 8. Aitoff projection of the MFB corrected distance sample in galactic coordinates (597 galaxies)

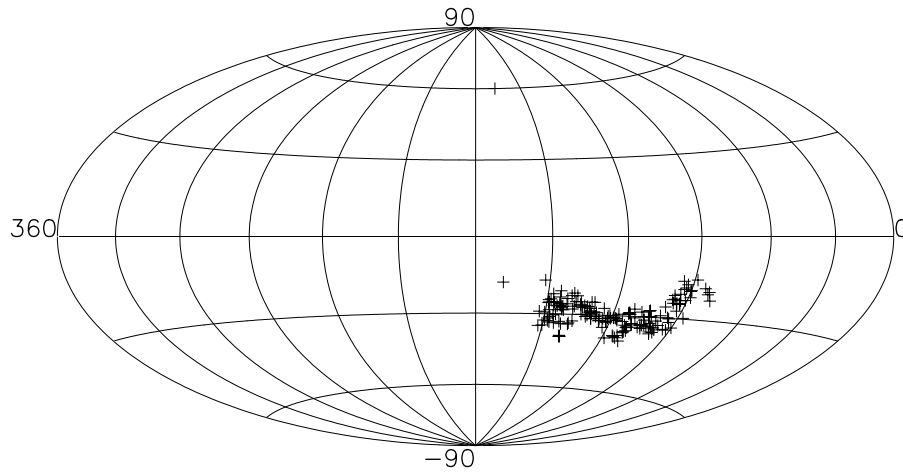


Fig. 9. Aitoff projection of the W91PP corrected distance sample in galactic coordinates (167 galaxies)

to 25%, depending on the passband) and forces us to smooth the derived peculiar velocity field for extracting reliable informations.

Fig. 10 shows the Hubble diagram obtained from the KLUN sample, together with the average points $\langle d_{corr} \rangle(V)$ (open circles, upper panel) and $\langle V \rangle(d_{corr})$ (open squares, lower panel). The first series of points follows quite well the uniform Hubble law up to a distance of 130-140 Mpc. These points are sta-

tistically correct, given the construction of the corrected distance scale, because corrected distances d_{corr} were built so that $\langle V/d_{corr} \rangle = H_0$ for every normalized distance d_n , and consequently for every kinematical distance d_{kin} or radial velocity V_{rad} . In this way $\langle d_{corr} \rangle = \langle d_{true} \rangle$ whatever the radial velocity. This last assertion is not valid with the second series of mean points, because corrected distances are correct "on average", and in principle, they cannot be used as "individual" distances,

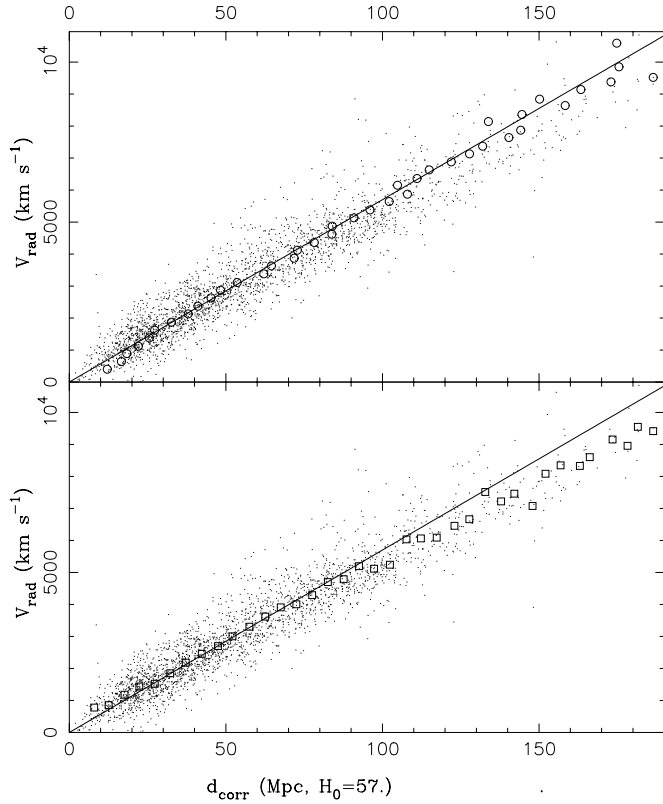


Fig. 10. Hubble diagram obtained from the KLUN sample. Radial velocity corrected for a Virgo infall component is plotted against the corrected TF distance. On top panel, the open circles represent the mean points $\langle d_{corr} \rangle(V)$ obtained within bins of 250 km s^{-1} ; on bottom panel, the open squares represent the mean points $\langle V \rangle(d_{corr})$ obtained within bins of 5 Mpc . The straight line corresponds to $H_0 = 57 \text{ km s}^{-1} \text{ Mpc}^{-1}$

for binning the distance axis. Moreover, they suffer from what could be called a “Gould effect” (Gould, 1993) due to a selection effect in redshift space: beyond $V \simeq 8000 \text{ km s}^{-1}$ redshifts measurements are lacking, and $\langle V \rangle(d_{corr})$ diverges beyond $d \simeq 100 \text{ Mpc}$ (see Fig. 10).

5.2. V vs. d diagram in the direction of a cluster

Our bias correction method assumes that in first approximation the kinematical distance well represents the true distance of a galaxy, i.e. that the velocity field is a pure Hubble flow. This is no more true if the galaxy takes part in a bulk motion like an infall motion toward the center of a cluster. When approaching the cluster from its front side, observed radial velocities of galaxies become greater and greater with respect to their cosmic component $H_0 d$; when going away from the back side of the cluster, observed radial velocities of galaxies become smaller than their cosmic component. As a consequence, when approaching a cluster, we tend to over-correct TF distances (the true distance is overestimated); and when going away beyond the cluster, we tend to under-correct TF distances (the true distance is under-estimated). Translated in terms of peculiar velocities,

this means that the observed infall amplitude traced by the series $\langle d_{corr} \rangle(V)$ is reduced, compared to the true infall motion. On the other hand, if such an infall pattern is observed (the typical “S-curve”), we are sure of the existence of an important mass overdensity in the region sighted.

Concerning the second series of points ($\langle V \rangle(d_{corr})$), the observed infall pattern is strongly biased by the convolution of the galaxy density gradient (due to the cluster) and the distribution function of the TF residuals. The overdensity region appears more extended, and the infall motion is magnified by the bias. It has the advantage of revealing infall motions, even of small amplitudes, and the location of their center.

We give below two examples of kinematical study in the direction of the Perseus-Pisces supercluster and toward the Great Attractor.

5.3. An infall pattern in the Perseus-Pisces region

The Perseus-Pisces (PP) supercluster is a massive, filamentary structure concentrated at a redshift of about 5000 km s^{-1} in the direction $(l, b) \sim (120^\circ, -30^\circ)$ (Haynes&Giovanelli,1988). The deepness of the KLUN sample (redshifts up to $10,000 \text{ km s}^{-1}$) covering a wide solid angle, is particularly well adapted for studying peculiar velocities in this region, which is rich in spiral galaxies.

The Perseus-Pisces region has been studied by numerous authors, without any definitive conclusion about a possible bulk flow of galaxies in its direction, though it is a prominent feature of our Local Universe. However, on the basis of a sample of 274 spiral galaxies spanning the right ascension range $21^h 40^m - 4^h$ and the declination range $21.5^\circ - 33.5^\circ$, Willick (1990) concluded that the region can be described by small scale motions, most likely due to the pull of the PP filament and the push of the foreground void, superposed on a large scale flow revealed by an excess of negative peculiar velocities. This overall motion of galaxies in PP, was found to be in about the same direction as the large scale flow modeled by the Great Attractor. On the basis of the same sample, but using a different method based on Monte-Carlo simulations for controlling biases, Freudling et al. (1995) revealed a significant infall into the PP supercluster complex. This result was further confirmed by Da Costa et al. (1996) from a whole sky sample of 1300 field galaxies. An other study by Han & Mould (1992), on the basis of 21 clusters distributed on the whole sky (among them five in the direction of PP), showed that the kinematics of our Local Universe can be described by a model in which galaxies are infalling to two mass concentrations, one in PP and one in Hydra-Centaurus. Finally, this region was studied recently by Hudson et al. (1998), using the inverse Fundamental Plane (FP) relation and a set of 103 ellipticals distributed in several clusters. For one of the background clusters, these authors evidenced a marginal backside infall toward the center of the PP complex, the latter being found roughly at rest with respect to the CMB frame.

We show in Fig. 11 the Hubble diagram obtained with the KLUN corrected distance sample in the direction of PP. The region surveyed covers the area $(90^\circ < l < 155^\circ; -45^\circ < b <$

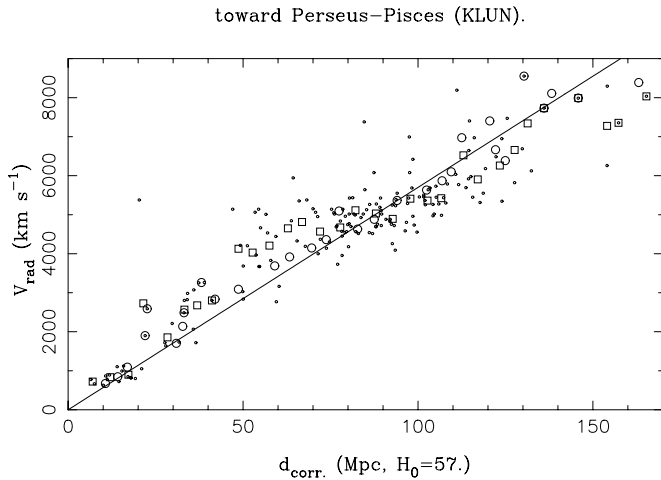


Fig. 11. Hubble diagram obtained from the KLUN sample, in the direction of the **Perseus-Pisces** supercluster (see text). Radial velocity corrected for a Virgo infall component is plotted against the corrected TF distance. The open circles represent the mean points $\langle d_{corr} \rangle(V)$ obtained within bins of 250 km s^{-1} ; the open squares represent the mean points $\langle V \rangle(d_{corr})$ obtained within bins of 5 Mpc. The straight line corresponds to $H_0 = 57 \text{ km s}^{-1} \text{ Mpc}^{-1}$

-15°). Open circles and open squares correspond to the mean points described in Sects. 5.1. and 5.2.. A large amplitude infall pattern is clearly revealed by the two sets of points, exhibiting for the first time both front-side and back-side infalls. According to the discussion of Sect. 5.2, the true "S-curve", corresponding to the true density distribution, is somewhere between the two patterns traced by the two series of points.

A similar result is obtained with the r -band W91PP sample (Fig. 12), even if this sample covers a too narrow area on the sky for actually tracing the infall motion in the surroundings of the PP supercluster. In addition, a non negligible part of the objects belongs to the triple value region, and disturb the pattern. However, due to the smaller scatter of the TF relation in r -band, the "open square curve" is here less affected by the bias than with the KLUN B -band sample.

The center of the infall is located at $d \simeq 90 \text{ Mpc}$ or $V_{rad} \simeq 4850 \text{ km s}^{-1}$, and the dynamical influence extends from $\sim 40 \text{ Mpc}$ up to $\sim 140 \text{ Mpc}$. This large scale flow is probably not only due to the PP supercluster, but also to the gravitational pull of numerous dense clusters in the surveyed region (Pegasus and A400 clusters are for example located close to the PP direction).

5.4. On the Great Attractor debate

The existence of a Great Attractor dominating the kinematics of the Local Universe has been a long and controversial debate. First report on a large scale coherence in the field of peculiar velocities goes back 10 years ago, with a paper from Dressler et al. (1987). The authors showed evidence that galaxies over a large volume of space share the Local Group's motion of $\sim 600 \text{ km s}^{-1}$ with respect to the microwave background radiation. Lynden-Bell et al. (1988) proposed a model where the appar-

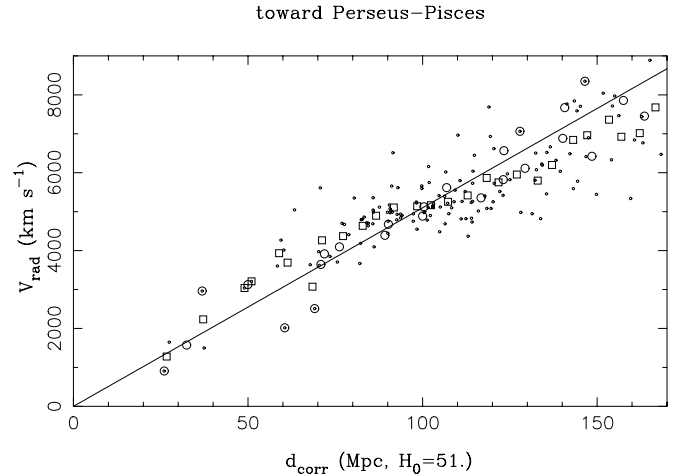


Fig. 12. Hubble diagram obtained from the W91PP sample (see text and Fig. 9). Radial velocity corrected for a Virgo infall component is plotted against the corrected TF distance. Open circles, and open squares are defined as in Fig. 11. The straight line corresponds to $H_0 = 51 \text{ km s}^{-1} \text{ Mpc}^{-1}$

ently high-amplitude bulk flow was due to the gravitational pull of a so-called Great Attractor, an extended overdense region centered at $\sim 4300\text{-}4500 \text{ km s}^{-1}$ in the direction $(l, b) \sim (307^\circ, 9^\circ)$. More extensively, this region includes the Hydra-Centaurus supercluster and some important concentrations in Pavo-Indus and Antlia. The GA model became a challenge to structure formation model based on hot or cold dark matter, both unable to generate such large fluctuations in the mass distribution.

Another difficulty comes from the fact that the putative center of this attractor is close to the Galactic plane in a region where dust and gas hide background galaxies when observing in the usual passbands B and V . Thanks to some recent and systematic blind surveys at 21-cm in this zone (e.g. Kraan-Korteweg, 1996; Bottinelli et al. 1993), which have searched for the mass counterpart responsible for the observed flow. These investigations have revealed some new extragalactic features, such as the Puppis cluster and Abell 3627 cluster, accounting for at most 10% of the mass required by the GA model.

Note that a variant of the GA model has been proposed by several authors (Mathewson et al. 1992b, Rauzy et al. 1992, Willick 1990), concluding that our local region and the GA itself could take part in a larger scale but constant velocity field.

We show in Fig. 13 the Hubble diagram obtained with the KLUN corrected distance sample in the direction of the GA. As in Mathewson et al. (1992b), the region surveyed covers the sky area $(260^\circ < l < 330^\circ; -40^\circ < b < +45^\circ)$. Unfortunately, due to large extinction effects in B -band and consequently large uncertainties on magnitude, objects belonging to the Zone of Avoidance (i.e. the area 15° appart from the Galactic plane) have been excluded, and the region is consequently poorly sampled. However, the large bulk flow implied by the GA should be well revealed by this plot, especially because the noisy triple value region has been naturally excluded by the selection. Indeed, such a large flow is not evidenced by our KLUN sample, and only a

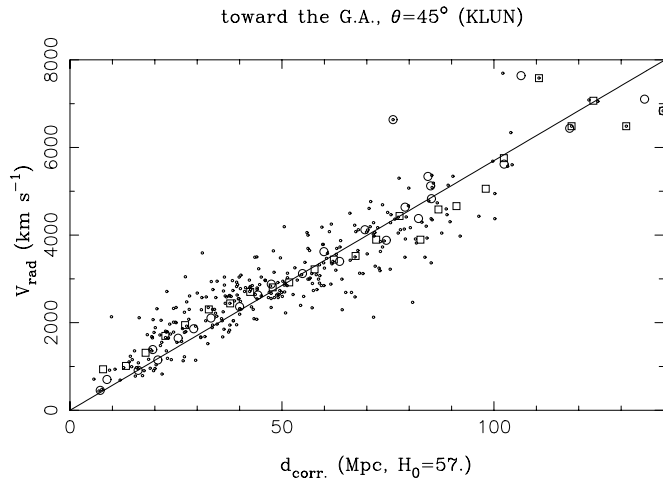


Fig. 13. Hubble diagram obtained from the KLUN sample, in the direction of the putative GA ($260^\circ < l < 330^\circ$; $-40^\circ < b < +45^\circ$). Radial velocity corrected for a Virgo infall component is plotted against the corrected TF distance. Open circles, and open squares are defined as in Fig. 11. The straight line corresponds to $H_0 = 57 \text{ km s}^{-1} \text{ Mpc}^{-1}$

hint of infall pattern can be guessed, centered roughly around a redshift of 3000 km s^{-1} . This redshift range is compatible with the location of the Hydra-Centaurus complex, which is contained in the area investigated. Nothing is detected at the expected redshift of 4500 km s^{-1} .

This result is confirmed by a study of the same region with the MFB *I*-band sample which extends closer to the Galactic plane (down to $|b| = 8^\circ$). Fig. 14 shows the Hubble diagram in the direction of the GA, for two different solid angle around its center ($\theta < 45^\circ$ and $\theta < 25^\circ$). Thanks to the smaller TF scatter in *I*-band, and a better sampling of the area, a clear though small amplitude infall pattern is seen on both panels. The infall center corresponds in both panels to a redshift of $\sim 3000 \text{ km s}^{-1}$. However, a second possible center is seen on the top panel (for a larger sky coverage) at a redshift of $\sim 4200 \text{ km s}^{-1}$ ($d \sim 62 \text{ Mpc}$, $H_0 = 51$). Contrarily to the conclusions by Mathewson et al. (1992) with the same sample, a significant backside infall is detected up to redshifts of 6000 km s^{-1} . Rather than a great attractor, the results are in better agreement with a cumulative pull of the numerous mass concentrations roughly aligned in this direction, reinforcing the conclusions by Federspiel et al. (1994).

Mathewson et al. (1992b) did not detect any backside infall, but a large bulk flow with large positive peculiar velocities up to the limit of the sample. Thanks to the good quality of their data, and of the use of the less scattered *I*-band TF relation, the authors claimed that the classical GA model of a large convergent flow was definitely ruled out. They used the TF relation as distance criterion, and corrected their derived distances from the Malmquist bias of the first kind (Teerikorpi 1994, 1997) by applying to the whole sample a correction factor of 8% deduced from the classical Malmquist formula $\Delta M = 1.382\sigma^2$.

We recall that this kind of correction is valid only in the case of a homogeneous spatial distribution of galaxies. However, it

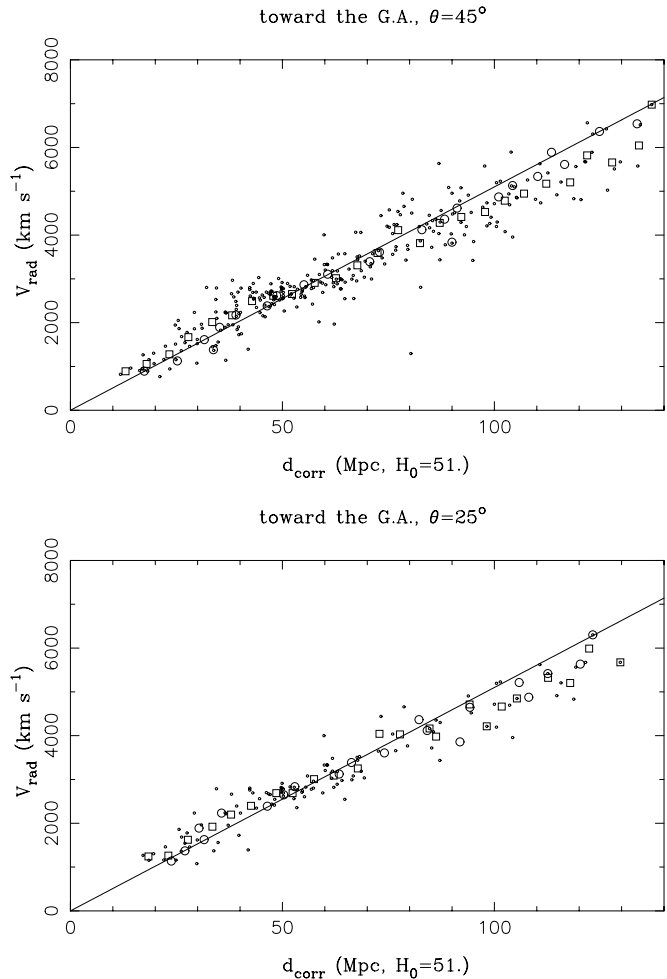


Fig. 14. Hubble diagram obtained from the MFB sample (see Fig. 8) for two solid angle ($\theta < 45^\circ$ and $\theta < 25^\circ$) around the GA direction ($l, b = (307^\circ, 9^\circ)$). Radial velocity corrected for a Virgo infall component is plotted against the corrected TF distance. Open circles, and open squares are defined as in Fig. 11. The straight line corresponds to $H_0 = 51 \text{ km s}^{-1} \text{ Mpc}^{-1}$

is free from selection effects on magnitudes, and thus does not require the extraction of a strictly magnitude limited sample. These corrected distances $d_{hom.} = d_{TF} \exp(\frac{7}{2}\alpha^2\sigma_{TF}^2)$ are unbiased in the sense that for a given $d_{hom.}$, i.e. for a given couple (m, p) , the mean true distance is equal to $d_{hom.}$. It is then the mean points $\langle V \rangle (d_{hom.})$ which trace either the Hubble law, or the infall pattern we are interested in. Moreover, if one instead uses the other series of mean points $\langle d_{hom.} \rangle (V)$, one gets negative peculiar velocities at short distances and positive peculiar velocities at large distances, because for a fixed true distance d_{true} , $d_{hom.}$ overestimates d_{true} at short distances and under-estimates d_{true} at large distances. Indeed, the bias $\langle \log d_{hom.} \rangle - \log d_{true} \simeq \frac{7}{2}\alpha\sigma_{TF}^2 - 0.2C(\omega(d_n))$ (cf Sect. 3) depends differentially on the true distance, i.e. on the redshift, and also on the completeness limit of the sample.

We plotted on Fig. 15 the Hubble diagram in the direction of the Great Attractor region, using for the TF scatter σ_{TF} the

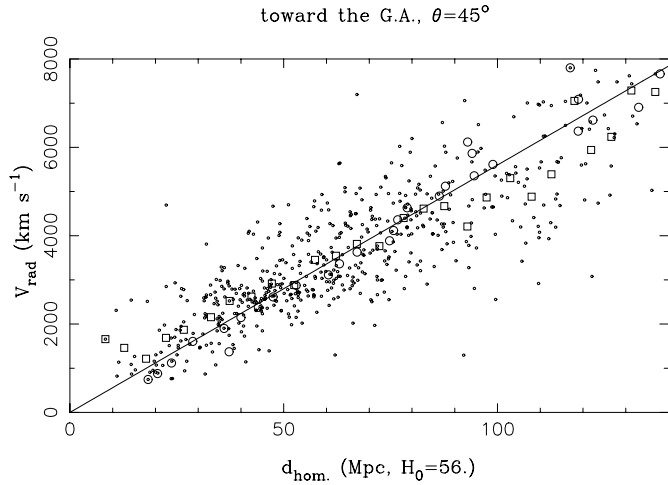


Fig. 15. Hubble diagram obtained from the MFB sample (within a solid angle $\theta < 45^\circ$ around $(l, b) = (307^\circ, 9^\circ)$ in the GA direction, when using the homogeneous Malmquist correction factor. Open circles, and open squares are defined as in Fig. 11. The straight line corresponds to $H_0 = 56 \text{ km s}^{-1} \text{ Mpc}^{-1}$

observed value of 0.43, which leads to a homogeneous correction of 14.7% on TF distances. Even if more scattered than in Fig. 14, the plot indicates three possible centers of infall at $V \sim 3000 \text{ km s}^{-1}$, $V \sim 3700 \text{ km s}^{-1}$, and $V \sim 4500 \text{ km s}^{-1}$ as traced by the open squares. The Hubble constant H_0 estimated using these corrections is also slightly different from the one estimated from the unbiased part only (56 instead of 51 $\text{km s}^{-1} \text{ Mpc}^{-1}$ with the NDM method). These value is less sensitive to the influence of peculiar velocities, but it is valid only under the assumption of the homogeneity of the galaxies space distribution.

Notice that using a TF scatter of 0.32 mag, derived from TF regressions in clusters (where selection effects reduce the observed magnitude dispersion), Mathewson et al. (1992b) have under-estimated the effect of the Malmquist bias, and then under-estimated the correction to be applied. Moreover, because they sliced their plot (in their Fig. 1) into horizontal bins, i.e. according to redshifts, they obtained a biased sequence of points (the open circles in Fig. 15) that diverges toward spurious positive peculiar velocities at large distances, and hides any backside infall behind the GA region.

6. Conclusions and further prospects

In the present paper, we address the problem of TF calibration and distance determination using a strictly apparent magnitude or diameter complete sample. On the basis of a safe statistical analysis, we show that:

- In contrary to other standard technics, the NDM calibration step does not require any bias correction, i.e. thanks to the introduction of normalized distances, we extract from the parent sample an unbiased subsample (the plateau data) for which the galaxy distribution in the (M, p) plane of the TF relation is not truncated by selection effects.

- The method allows us to define an unbiased distance indicator valid for the whole parent sample, as long as completeness in magnitude (resp. in apparent diameter) is verified.
- This NDM distance indicator is robust since no assumption is required neither on the spatial density distribution of the galaxies, nor on the p and luminosity distribution functions. In addition, this distance estimate is also independent of selection effects in p and distance modulus μ .

A first application of this new tool to kinematical analysis leads to the following results:

- We showed evidence for a large amplitude convergent flow in the direction of the Perseus-Pisces supercluster. For the first time, thanks to our reliable correction method, a backside infall was detected.
- The expected large convergent infall toward the putative "Great Attractor" was not confirmed, neither a large constant bulk flow in the same direction proposed by some authors. However, centers of infall were clearly detected, in the region $(260^\circ < l < 330^\circ; -40^\circ < b < +45^\circ)$, and it seems that the peculiar velocity field may be essentially described by the cumulative pull of several structures such as Hydra-Centaurus complex, Antlia and Pavo-Indus clusters.

Our kinematical study set the preliminary steps of a more general dynamical analysis, where the method will be applied to various mass concentrations. Tolman-Bondi simulations will allow us to compare the derived infall pattern (for different angular distances from the infall center) with theoretical "S-curves", providing us with informations on cluster mass distribution and cluster mass-to-light ratio (Hanski et al. in preparation).

Peculiar velocity field reconstruction, such as POTENT (see e.g. Dekel, 1994), still requires a large and homogeneous all sky TF sample with reduced distance uncertainties. This should be achieved in the next years with current NIR surveys such as DENIS and the associated spectrometric programmes 6dF (6 degree Field multi-fibers spectrograph) and FORT-Key-project (with the refurbished Nançay radiotelescope).

References

- Bottinelli, L., Gouguenheim, L., Paturel, G., Teerikorpi, P., 1986, A&A 156, 157
- Bottinelli, L., Gouguenheim, L., Fouqué P., Paturel, G., 1990, A&AS 82, 391
- Bottinelli, L., Durand, N., Fouqué P. et al., 1992, A&AS 93, 173 (paper I)
- Bottinelli, L., Durand, N., Fouqué P. et al., 1993, A&AS 102, 57 (paper II)
- Bottinelli, L., Gouguenheim, L., Paturel, G., Teerikorpi, P., 1995, A&A 296, 64
- Burstein, D., Heiles, C., 1984, ApJS 54, 33
- Da Costa, L.N., Freudling, W., Wegner, G. et al., 1996, ApJ 468, L5
- Dekel, A., 1994, ARA&A 32, 371
- Di Nella, H., Paturel, G., Walsh, A. et al, 1996, A&ASS 118, 311
- Dressler, A., Faber, S., Burstein, D. et al., 1987, ApJ 313, L37
- Ekholm, T., Teerikorpi, P., 1994, A&A 284, 369
- Federspiel, M., Sandage, A., Tammann, G.A., 1994, ApJ 430, 29

- Fouqué P., Paturel, G., 1985, A&A 150, 192
Freudling, W., Da Costa, L.N., Wegner, G. et al., 1995, AJ 110, 920
Giovannelli, R., Haynes, M.P., 1985, AJ 90, 2445
Giovannelli, R., Myers, S.T., Roth, J., Haynes, M.P., 1986, AJ 92, 250
Giovannelli, R., Haynes, M.P., Herter, T. et al., 1997, AJ 113, 53
Gould, A., 1993, ApJ 412, L55
Han, M., Mould, J.R., 1992, ApJ 396, 453
Hanski, M. et al. 1998, A&A in preparation
Haynes, M.P., Giovannelli, R., 1988, in Large-scale motions in the Universe, Princeton University Press, pp 31-70
Hudson, M.J., Lucey, J.R., Smith, R.J., Steel, J., 1997, MNRAS 291, 488
Kraan-Korteweg, R., Woudt, P.A., Cayatte, V., Fairall, A.P., Balkowski, C., Hemming, P.A., 1996, Nature 379, 519
Lynden-Bell, D., Faber, S., Burstein, D. et al., 1988, ApJ 328, 19
Mathewson, D.S., Ford, V.L., Buchhorn, M., 1992a, ApJS 81, 413 (MFB)
Mathewson, D.S., Ford, V.L., Buchhorn, M., 1992b, ApJ 389, L5
Mould, J. et al. 1980, ApJ 238, 458
Paturel, G., Petit, C., Kogoshvili, N., et al., 1991, A&ASS 91, 371
Paturel, G., di Nella, H. Bottinelli, L. et al, 1994, A&A 289, 711 (paper III)
Paturel, G., Garnier, R., Petit, C., Marthinet, M., 1997a, A&A 311, 12
Paturel, G., Andernach, H., Bottinelli, L. et al., 1997b, A&ASS 124, 109
Peebles, P.J.E., 1976, ApJ 205, 318
Rauzy, S., 1997, A&ASS 125, 255 (astro-ph/9701184)
Rauzy, S., Lachièze-Rey, M., Henriksen, R.N., 1992, A&A 256, 1
Rauzy, S., Triay, R., 1996, A&A 307, 726
Sandage, A., 1994, ApJ 430, 1
Schneider, D.P., Gunn, J.E., Hoessel, J.G., 1983, ApJ 264, 337
Teerikorpi, P., 1984, A&A 141, 407
Teerikorpi, P., 1993, A&A 280, 443
Teerikorpi, P., 1995, Astrophys. Lett. Comm. 31, 263
Teerikorpi, P., 1997, ARA&A 35, 101
Theureau, G., 1998, A&A 331, 1 (paper VI)
Theureau, G., Hanski, M., Teerikorpi, P. et al., 1997a, A&A 319, 435 (paper IV)
Theureau, G., Hanski, M., Ekholm, T. et al., 1997b, A&A 322, 730 (paper V)
Theureau, G., Bottinelli, L., Coudreau-Durand, N. et al., 1998a, A&ASS 130, 333 (paper VII)
Theureau, G., Lanoix, P., Musella, I., 1998b, A&A in preparation
Triay, R., Lachièze-Rey, M. Rauzy, S., 1994, A&A 289, 19
Triay, R., Rauzy, S., Lachièze-Rey, M., 1996, A&A 309, 1
Willick, J.A., 1990, ApJ 351, L5
Willick, J.A., 1991, Ph.D. Thesis, Univ. of California, Berkeley (W91PP)
Willick, J.A., Courteau, S., Faber, S.M. et al., 1997, APJS 109, 333
Yahil, A., Tammann, G., Sandage, A., 1977, ApJ 217, 903